Research Square

Preprints are preliminary reports that have not undergone peer review.
They should not be considered conclusive, used to inform clinical practice,
or referenced by the media as validated information.

Rainfall Variability, Season Timing, and Dry-Spell Risk at Somanya, Eastern Ghana (1996 to 2025): Implications for Rain-Fed Agriculture

Michael Akosey

makosey@gs.uesd.edu.gh

University of Environment and Sustainable Development

Jessica Amu

University of Environment and Sustainable Development

Fatima Eshun

University of Environment and Sustainable Development

Sarfo Okyere Kore

University of Environment and Sustainable Development

Bernard Akowuah

University of Environment and Sustainable Development

Maximillian-Robert Selorm Doku

University of Environment and Sustainable Development

Research Article

Keywords: bimodal regime, Mann-Kendall, Sen's slope, Standardized Precipitation Index, CHIRPS validation, ENSO teleconnection, return periods, onset and cessation, West Africa

Posted Date: November 12th, 2026

DOI: https://doi.org/10.21203/rs.3.rs-11360581/v1

License: This work is licensed under a Creative Commons Attribution 4.0 International License.
Read Full License

Additional Declarations: No competing interests reported.

Rainfall Variability, Season Timing, and Dry-Spell Risk at Somanya, Eastern Ghana (1996 to 2025): Implications for Rain-Fed Agriculture

Michael Akosey[a, *], Jessica Amu[a], Fatima Eshun[a], Sarfo Okyere Kore[a], Bernard Akowuah[a], Maximillian-Robert Selorm Doku[a]

[a] *University of Environment and Sustainable Development, Somanya, Ghana*

Corresponding author*: Michael Akosey, University of Environment and Sustainable Development, Somanya, Ghana. Email: makosey@gs.uesd.edu.gh*

Abstract

Many farming districts in southern Ghana, Somanya among them, are uncharacterized and rely on regional generalisations that may not hold locally. A complete daily rainfall record for Somanya (1996 to 2025) was analysed for regime, season timing, trend and abrupt change. Totals, rainy days, onset and cessation, dry spells, extreme-rainfall, concentration and seasonality indices, and the Standardized Precipitation Index (SPI) were computed. Trend and homogeneity used the Mann-Kendall, Sen's slope and Pettitt tests, and the gauge was validated against CHIRPS ($r = 0.90$ monthly; about 5 percent bias). Mean annual rainfall is 1,187 mm at a coefficient of variation of 11.1 percent, among the more dependable in the south. The regime is bimodal, peaking in June and October around the August dry spell (Seasonality Index 0.46). No index shows a significant trend and the series is homogeneous. Two structural signals favour farming: earlier major-season onset (about 0.6 days per year, $p = 0.16$) and fewer spells of ten or more consecutive dry days ($p = 0.05$). The SPI marks 2015 to 2016 as the deepest drought and 2008 as the wettest year. Rainfall differs across El Nino-Southern Oscillation phases (one-way analysis of variance $p = 0.03$), La Nina years running wetter. A district grid places the gauge at the local mean within a west-to-east drying gradient. Planting should track observed onset rather than the calendar; dry-spell and spatial risk, not the annual total, deserve attention. This first CHIRPS-validated station assessment provides a baseline for local agricultural and water planning.

Keywords: *bimodal regime; Mann-Kendall; Sen's slope; Standardized Precipitation Index; CHIRPS validation; ENSO teleconnection; return periods; onset and cessation; West Africa*

1. Introduction

Farming decisions in West Africa turn on the weather, and rainfall matters more than any other variable. Across the region most food is grown without irrigation, so a good or bad year in the rains becomes a good or bad year in the harvest, in water availability, and in household income (Nicholson 2013; Sanogo et al. 2015). What sets the seasonal rhythm is the north-and-south migration of the Intertropical Convergence Zone (ITCZ) and the moisture-bearing south-westerly monsoon, which advances over the sub-region in the first half of the year and retreats after mid-year (Omotosho and Abiodun 2007; Nicholson 2013). On top of that seasonal cycle sits strong year-to-year and decadal variability, and mounting evidence that a warming climate is changing how often and how hard both wet and dry extremes strike West Africa (IPCC 2021; Atiah et al. 2020). None of this is abstract for people whose calendars are built around the rains. A late start, a longer break in mid-season, or a single violent downpour can be the difference between a crop and a loss.

The same convergence-zone migration splits Ghana in two: a single wet season in the north, and in the south a bimodal regime made of a major season, a short mid-year dry spell, and a minor season (Dickson and Benneh 1988; Ofori-Sarpong and Annor 2001). In that bimodal south, how a farming season turns out depends less on the yearly total than on the internal shape of the rains, on when each season opens and closes, how long the dry spells inside it run, and how the heaviest days fall (Stern et al. 1982; Amekudzi et al. 2015; Usman and Reason 2004). A season of average total can still fail when a long break lands on flowering, and an otherwise wet year can still flood when its rain arrives in a handful of intense events (Ansah et al. 2020; Ackom et al. 2020).

Study of West African rainfall has moved quickly since the Sahel droughts of the 1970s and 1980s, which gave way to a partial, patchy recovery from the 1990s onward (Nicholson 2013; De Longueville et al. 2016; Sanogo et al. 2015). The Ghanaian picture is one of weak, spatially variable trends. Owusu and Waylen (2009) documented strong spatio-temporal variability in annual rainfall over 1951 to 2000. Lacombe et al. (2012), applying a resampling-based Mann-Kendall test across sixteen stations, showed that trends significant at the regional scale mostly vanished at individual stations, and pointed instead to structural change, delayed onset and lengthening dry spells. Logah et al. (2013) described a broad decline, with the wettest zones shifting south-westward. Newer station and basin work leans the other way, toward stabilisation or mild recovery in the south. Ackom et al. (2020) reported a non-significant positive annual trend and a significant dry-season increase in the Odaw basin near Accra; Braimah et al. (2022) found rising minor-season rainfall at sixteen of seventeen southern stations; and Kabo-Bah et al. (2016), Nyatuame et al. (2014), and Baidu et al. (2017) found mostly weak or oscillatory behaviour elsewhere. The agronomic and extreme side has

grown alongside, with Amekudzi et al. (2015) mapping onset, cessation, and season length across the agro-ecological zones and Atiah et al. (2020) analysing ETCCDI extreme indices nationally from CHIRPS and tying them to sea-surface-temperature forcing. Underneath all of it sits a shared non-parametric toolkit, the Mann-Kendall test (Mann 1945; Kendall 1975), the Sen's slope estimator (Sen 1968), the Pettitt change-point test (Pettitt 1979), the Standardized Precipitation Index (McKee et al. 1993), and the ETCCDI indices (Zhang et al. 2011), and, where gauge networks are sparse, validated satellite-gauge products such as CHIRPS (Funk et al. 2015; Dinku et al. 2018).

Three gaps run through this literature. First, the Ghanaian evidence leans heavily on regional and national analyses built from gridded products or clusters of stations. Their spatial averaging smooths away the local detail that decides what happens on a given farm, so a trend that is significant once pooled regionally is frequently absent at the individual station (Lacombe et al. 2012; Owusu and Waylen 2009; Atiah et al. 2020). Second, the variables that matter most to rain-fed agriculture, the onset and cessation of the seasons, dry-spell length and frequency, extreme daily rainfall, and drought, are seldom studied together for one place over a long daily record; they tend to be taken one or two indices at a time, even though it is their combination, not any single index, that governs planting decisions and crop risk (Stern et al. 1982; Usman and Reason 2004; Amekudzi et al. 2015). Third, when a single gauge is used, its spatial representativeness is usually assumed rather than shown, even though validated gridded products now make that test straightforward (Funk et al. 2015; Dinku et al. 2018).

For Somanya these gaps bite. It is a farming town in the coastal-savanna transition of the Eastern Region, on the drier margin of the bimodal south, where the two rain-fed seasons run shorter and less dependably than in the forest belt to the west (Dickson and Benneh 1988; Ofori-Sarpong and Annor 2001), and where the surrounding area has seen both damaging floods and drought in recent years (Ansah et al. 2020; Ackom et al. 2020). The station holds an unusually complete thirty-year daily record, yet it has never been characterized in the published literature, so local decisions about planting calendars, small-reservoir and well storage, and flood risk still rest on regional generalisations that may not hold here. A station-scale baseline, framed agronomically and validated independently, is the missing first step. It tells the district's farmers when the seasons can be expected to begin and end, how often damaging mid-season dry spells occur, how large the design rainfall for local drainage is, and how far conditions vary across the municipality, none of which a national study can answer reliably. And because the West African recovery has reached different places at different rates

(Sanogo et al. 2015; Nicholson 2013), only station-scale evidence can show whether, and how, it has reached this particular community.

This study therefore sets out to give the first integrated, CHIRPS-validated characterization of Somanya's rainfall regime, and to build an agronomically relevant baseline for local agricultural and water planning. The specific objectives are: (i) to characterize the annual and seasonal rainfall regime, its variability, and its concentration; (ii) to determine the onset, cessation, and length of the rainy period and quantify their reliability; (iii) to analyse the frequency and duration of dry spells within the rainy period; (iv) to compute the ETCCDI extreme-rainfall indices and their return levels; (v) to assess meteorological drought using the Standardized Precipitation Index at three timescales; and (vi) to test all series for trend, homogeneity, and robustness, validate the gauge against CHIRPS, map the surrounding rainfall gradient, examine the association with the El Nino-Southern Oscillation, and interpret the findings for rain-fed agriculture against the published record for southern Ghana.

2. Materials and Methods

2.1 Study area

Somanya is the capital of the Yilo Krobo Municipal District in the Eastern Region of Ghana. The town lies at approximately 6.10° N, 0.02° W, close to the Greenwich (prime) meridian (Eshun et al. 2023). It is a low-relief landscape of sandy and loamy soils, with a farming economy built on rain-fed maize, cassava, legumes, and horticulture. The climate is tropical, driven by moist south-westerly monsoon flow during the rains and by dry, dusty north-easterly harmattan winds in the main dry season (Dickson and Benneh 1988; Nicholson 2013). Its position in the coastal-savanna transition places it in the drier part of the bimodal south, similar in setting to the nearby Accra plains studied by Ofori-Sarpong and Annor (2001) and Ackom et al. (2020), which makes season timing and dry-spell behaviour especially consequential for local agriculture. The main source of household water supply is the national grid (Eshun et al. 2023).

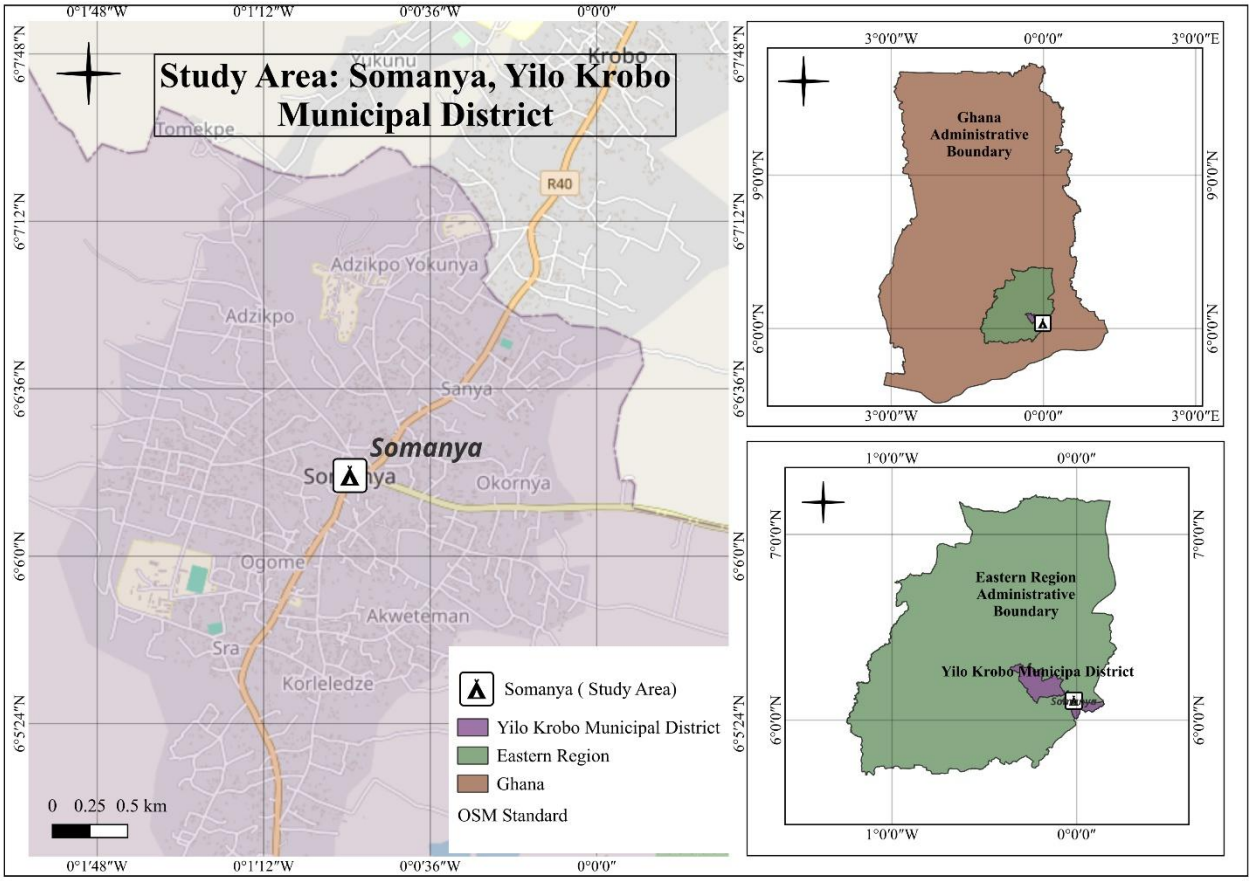


Figure 1: *Location of the study area, Somanya (6.10°N, 0.02°W), in the Yilo Krobo Municipal District, Eastern Region, Ghana*

2.2 Data and quality control

The dataset is a continuous daily rainfall series from 1 January 1996 to 28 February 2026, comprising 11,017 daily observations. All climatological and trend analyses were restricted to the 30 complete calendar years from 1996 to 2025, since the 2026 fragment covers only January and February and would bias annual and seasonal totals. Quality control confirmed a clean record with no missing entries and no negative values. The maximum recorded daily fall is 55.8 mm on 22 July 2017, consistent with heavy convective activity in the region.

To test how well the single gauge represents rainfall over its surroundings, the record was compared with the Climate Hazards Group InfraRed Precipitation with Station data (CHIRPS) version 2.0 (Funk et al. 2015), a blended satellite and station product at about 5.5 km resolution validated across sub-Saharan Africa (Dinku et al. 2018). Daily CHIRPS values were extracted for Somanya over 1996 to 2025 and compared with the gauge at daily, monthly, and annual scales using the Pearson and

Spearman correlation coefficients, percent bias (PBIAS), and the root mean square error, with agreement classified following the model-evaluation guidelines of Moriasi et al. (2007).

The agreement metrics are defined as follows, where Si is the CHIRPS estimate, Gi the gauge value, and n the number of paired observations:

$$\mathrm{PBIAS} = 100 \times [\Sigma(S_i - G_i) \,/\, \Sigma G_i] \qquad (1)$$

$$\mathrm{RMSE} = \sqrt{[\ (1/n)\ \Sigma(S_i - G_i)^2\ ]} \qquad (2)$$

2.3 Rainfall indices and seasonality

Rainfall was aggregated to annual totals, monthly climatological means, and seasonal totals, grouped operationally into a major wet period (March to July), a minor wet period (August to November), and a dry period (December to February) for the seasonal trend tests. A rainy day was defined as a day receiving at least 1 mm, and rainfall intensity was measured by the simple daily intensity index (SDII), the annual total divided by the number of rainy days (Zhang et al. 2011). Interannual variability was summarised with the coefficient of variation. The seasonal distribution of rainfall was described with the Precipitation Concentration Index of Oliver (1980), where values below 10 indicate uniform distribution, 11 to 15 moderate concentration, and 16 to 20 irregular distribution, and the Seasonality Index of Walsh and Lawler (1981), where 0.20 to 0.39 describes an equable climate, 0.40 to 0.59 a moderately seasonal climate with a short drier season, and 0.60 to 0.79 a markedly seasonal climate.

These indices are defined below, where σ and $\bar{x}$ are the standard deviation and mean of the annual totals, P the total wet-day rainfall, Nw the number of wet days (≥1 mm), pi the rainfall in month i, xn the total for month n, and R the annual total:

$$\mathrm{CV} = (\sigma \,/\, \bar{x}) \times 100 \qquad (3)$$

$$\mathrm{SDII} = P \,/\, N_w \qquad (4)$$

$$\mathrm{PCI} = 100 \times [\Sigma_{i=1}^{12}\, p_i^2\ ] \,/\, [\ (\ \Sigma_{i=1}^{12}\, p_i\ )^2\ ] \qquad (5)$$

$$\mathrm{SI} = (1/R)\ \Sigma_{n=1}^{12}\ |\ x_n - R/12\ | \qquad (6)$$

2.4 Onset, cessation, and length of the rainy period

Major-season onset was defined agronomically, following the logic of Stern et al. (1982), as the first day after 1 February on which rainfall accumulated over three consecutive days reached at least 20 mm and was not followed by a dry spell exceeding nine days within the subsequent 21 days. This kind of rule guards against a false start that a single heavy shower would otherwise trigger. Cessation

was taken as the first day after 1 October beginning a 15-day window with less than 5 mm of total rainfall. The length of the rainy period is the interval between onset and cessation, spanning the August break embedded within it.

2.5 Dry spells and extreme indices

Dry-spell behaviour was described by the annual maximum number of consecutive dry days (CDD), the maximum number of consecutive wet days (CWD), and the number of dry spells of at least seven and at least ten days within the March to November rainy period (Usman and Reason 2004; Zhang et al. 2011). Extreme rainfall was quantified with a standard subset of the ETCCDI indices (Zhang et al. 2011): the annual maximum one-day and five-day totals (RX1day, RX5day); the count of days at or above 10 mm and 20 mm (R10mm, R20mm); and the very-wet and extremely-wet day totals (R95p, R99p). A wet day was defined as a day with rainfall of at least 1 mm, consistent with the SDII and rainy-day definitions above. The 95th and 99th percentiles used for R95p and R99p were computed empirically from the full set of wet days across the entire 1996 to 2025 base period, which serves as both the reference and the analysis period; the resulting thresholds are 18.9 mm and 25.3 mm. Because the record is complete, no missing-value treatment or infilling was required, and all indices were computed on calendar years.

Return levels of extreme daily rainfall were estimated by fitting the Gumbel (type I extreme value) and generalized extreme value (GEV) distributions to the series of annual maximum daily totals (Coles 2001). Goodness of fit was assessed with the Kolmogorov-Smirnov test, and 90 percent confidence intervals for the return levels were obtained by non-parametric bootstrap resampling of the annual maxima. In the expressions below μ is the location, σ the scale, and ξ the shape parameter, and the T-year return level is the quantile x for which F(x) = 1 − 1/T:

$$\mathrm{F}(x) = \exp\{-\exp[-(x-\mu)/\sigma]\} \qquad (7)$$

$$\mathrm{F}(x) = \exp\{-[1+\xi(x-\mu)/\sigma]^{-1/\xi}\} \qquad (8)$$

2.6 Standardized Precipitation Index

Meteorological drought was assessed using the Standardized Precipitation Index (McKee et al. 1993) at 3, 6, and 12-month accumulation scales. For each accumulation a gamma distribution was fitted to the calendar-month series, with the probability of zero handled explicitly, and the fitted cumulative probabilities were transformed to the standard normal. Following convention, SPI at or below -1.0

denotes moderate drought, at or below -1.5 severe drought, and at or below -2.0 extreme drought, with symmetric thresholds for wet conditions.

The gamma probability density fitted to each accumulation is given below, where α and β are the shape and scale parameters and Γ(α) is the gamma function. Because rainfall can be zero, the cumulative probability is H(x) = q + (1 − q)G(x), with q the probability of zero, and the SPI is the standard normal quantile of H(x), that is SPI = $\Phi^{-1}[H(x)]$:

$$g(x) = 1/(\beta^{\alpha}\,\Gamma(\alpha))\; x^{\alpha-1}\; e^{-x/\beta}, \quad x > 0 \qquad (9)$$

2.7 Trend, homogeneity, and robustness tests

Trend was assessed with the Mann-Kendall rank-based test (Mann 1945; Kendall 1975), which assumes no particular distribution and tolerates outliers, and trend magnitude was estimated with the Sen's slope estimator (Sen 1968). Ordinary least squares regression was run alongside as a cross-check on the annual series. Because positive serial correlation can inflate the apparent significance of the Mann-Kendall statistic, the annual series was also tested with the variance-corrected modified Mann-Kendall test of Hamed and Rao (1998), and its lag-1 autocorrelation was computed. Homogeneity and any abrupt shift in the mean were assessed using the non-parametric Pettitt change-point test (Pettitt 1979). Significance was evaluated at the 5 percent level throughout.

The Mann-Kendall statistic S and its variance are defined below, where xj and xk are data values at times j and k, n is the record length, and tp is the number of ties of extent p; the standardized test statistic Z follows, with the sign convention sgn(θ) = +1, 0, −1 for θ > 0, = 0, < 0. Sen's slope β is the median of all pairwise slopes, and the Pettitt change-point statistic K locates an abrupt shift in the mean:

$$S = \Sigma_{k=1}^{n-1}\,\Sigma_{j=k+1}^{n}\,\mathrm{sgn}(x_j - x_k) \qquad (10)$$

$$\mathrm{Var}(S) = [\; n(n-1)(2n+5) - \Sigma_p\, t_p(t_p-1)(2t_p+5)\;]\;/\;18 \qquad (11)$$

$$Z = (S-1)/\sqrt{\mathrm{Var}(S)} \text{ if } S>0;\;\; 0 \text{ if } S=0;\;\; (S+1)/\sqrt{\mathrm{Var}(S)} \text{ if } S<0 \qquad (12)$$

$$\beta = \mathrm{median}\;[\;(x_j - x_i)\;/\;(j-i)\;], \quad i<j \qquad (13)$$

$$K = \max_{1\le t<n} |\; U_{t,n}\;|, \quad U_{t,n} = \Sigma_{i=1}^{t}\,\Sigma_{j=t+1}^{n}\,\mathrm{sgn}(x_i - x_j) \qquad (14)$$

2.8 Association with the El Nino-Southern Oscillation

The link between interannual rainfall and the El Nino-Southern Oscillation was examined using the Oceanic Nino Index (ONI) of the NOAA Climate Prediction Center (NOAA CPC 2024). Each

calendar year was assigned an annual-mean ONI and classified as El Nino (ONI ≥ +0.5), neutral, or La Nina (ONI ≤ −0.5). The relationship was tested with the Pearson correlation between annual rainfall and annual-mean ONI and with a one-way analysis of variance comparing mean annual rainfall across the three phases, significance being judged at the 5 percent level.

2.9 Software and implementation

All analyses were performed in Python 3. The Mann-Kendall test, its Hamed and Rao modification, and Sen's slope were computed with the pymannkendall package; distribution fitting for the Standardized Precipitation Index and the extreme-value return levels, the bootstrap confidence intervals, and the ENSO correlation and analysis of variance used SciPy and NumPy; index calculation and temporal aggregation used pandas; CHIRPS data were retrieved and processed in Google Earth Engine; and all figures were produced with Matplotlib.

3. Results and Discussion

3.1 Annual regime and interannual variability

Over 1996 to 2025 mean annual rainfall is 1,187 mm, with a standard deviation of 132 mm and a coefficient of variation of 11.1 percent (Table 1, Figure 2). The wettest year, 2008, brought 1,452 mm; the driest, 2005, brought 982 mm. The station records 145 rainy days in an average year, ranging from 119 to 168 (Figure 3), at a mean intensity of 8.2 mm per rainy day. A coefficient of variation near 11 percent is low for the region. In most years the annual total lands within about 130 mm of the long-term average, so the water available for cropping is fairly predictable from one year to the next, without the wider swings reported elsewhere in the country. The contrast with other studies is clear. Ackom et al. (2020) found much larger coefficients of variation, 19.5 to 29.0 percent, for annual totals in the nearby Odaw basin; Braimah et al. (2022) reported the lowest amounts and the highest variability in the minor season along the eastern coast; and Owusu and Waylen (2009) found strong interannual and spatial swings in Ghanaian rainfall through the second half of the twentieth century. Somanya's mean falls inside the 760 to 1,200 mm range Ackom et al. (2020) reported for the Odaw basin and above the drier east-coast stations of Braimah et al. (2022), which fits its inland, transitional setting. For a district that plants twice a year, that dependability is an asset: it makes a whole year's cropping less likely to be undone by a rainfall deficit, and it leaves the annual total a weaker source of risk than the timing and distribution of the rain, which the following sections take up.

Table 1. Summary rainfall statistics for Somanya 1996 to 2025.

Statistic	Value	Notes
Mean annual rainfall	1,187 mm	30-year average
Standard deviation	132 mm	interannual spread
Coefficient of variation	11.1 %	low variability
Wettest / driest year	1,452 / 982 mm	2008 / 2005
Mean rainy days (≥1 mm)	145 days	range 119 to 168
Mean daily intensity (SDII)	8.2 mm/day	per rainy day
Precipitation Concentration Index	10.9	moderate concentration
Seasonality Index	0.46	moderately seasonal
Maximum daily rainfall	55.8 mm	22 July 2017

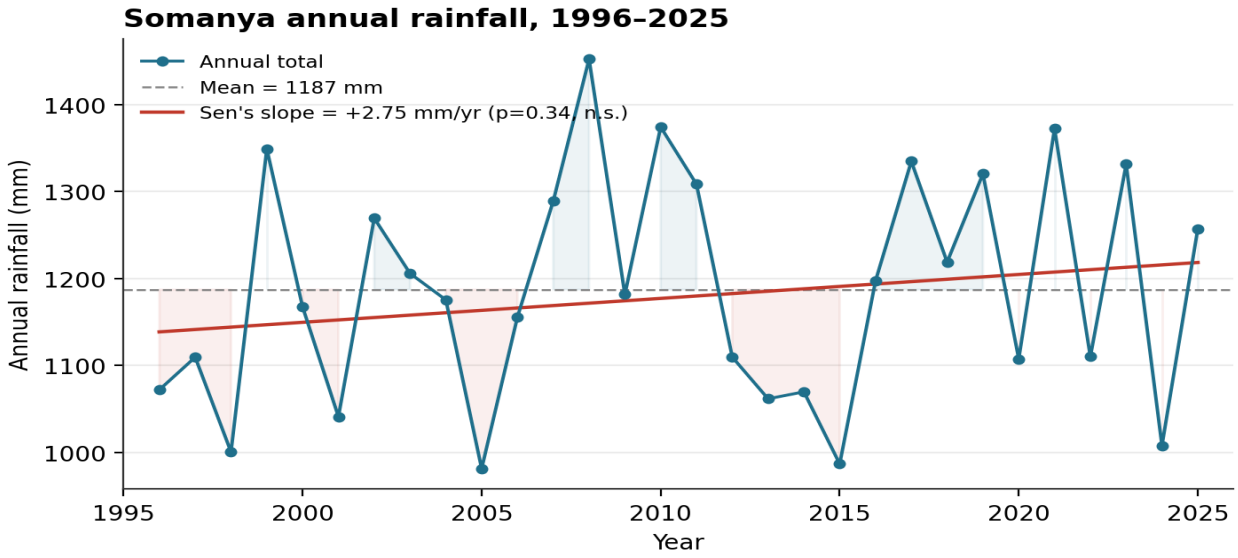


Figure 2. *Annual rainfall totals at Somanya 1996 to 2025, with the long-term mean and the Sen's slope estimate. The upward slope of 2.75 mm per year is not statistically significant.*

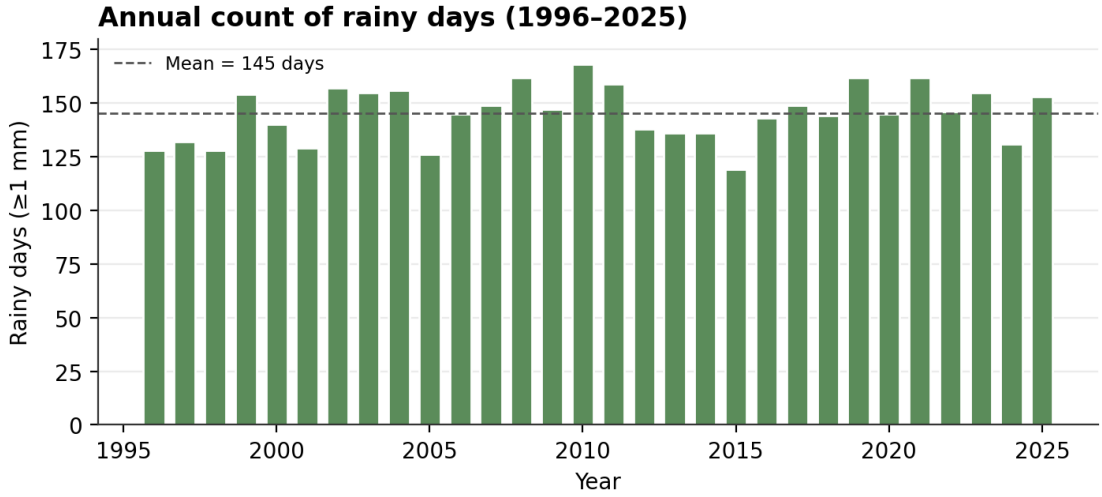


Figure 3. *Annual count of rainy days (at least 1 mm) with the long-term mean of 145 days. The mild upward tendency is not statistically significant.*

3.2 Seasonality and rainfall concentration

The monthly climatology has the double peak typical of southern Ghana (Figure 4). Rain builds from March to a major-season high near 182 mm in June, drops sharply to about 51 mm in August during the little dry season, then climbs to a second, lower peak of roughly 139 mm in October before the harmattan sets in from December. This is the coastal bimodal pattern first mapped by Dickson and Benneh (1988), quantified for nearby Accra by Ofori-Sarpong and Annor (2001), and reported for the Odaw basin by Ackom et al. (2020), all of whom put the major peak in June and the minor in October. Those studies used different data and different methods, gauge climatologies, gridded products, and wavelet decomposition, and still recovered the same seasonal structure. That agreement is a strength rather than a coincidence: the bimodal regime is a stable climatological feature imposed by the twice-yearly passage of the Intertropical Convergence Zone (Omotosho and Abiodun 2007; Nicholson 2013), so results that converge across methods build confidence rather than cast doubt. The strong annual periodicity Baidu et al. (2017) isolated by wavelet analysis is the spectral trace of the same cycle. The Precipitation Concentration Index averages 10.9 and the Seasonality Index 0.46, placing Somanya in the moderately seasonal band of Oliver (1980) and Walsh and Lawler (1981). Rainfall is spread across much of the year rather than bunched into a short wet spell, and that two-season shape is what cushions the annual total and gives the district two cropping windows instead of one.

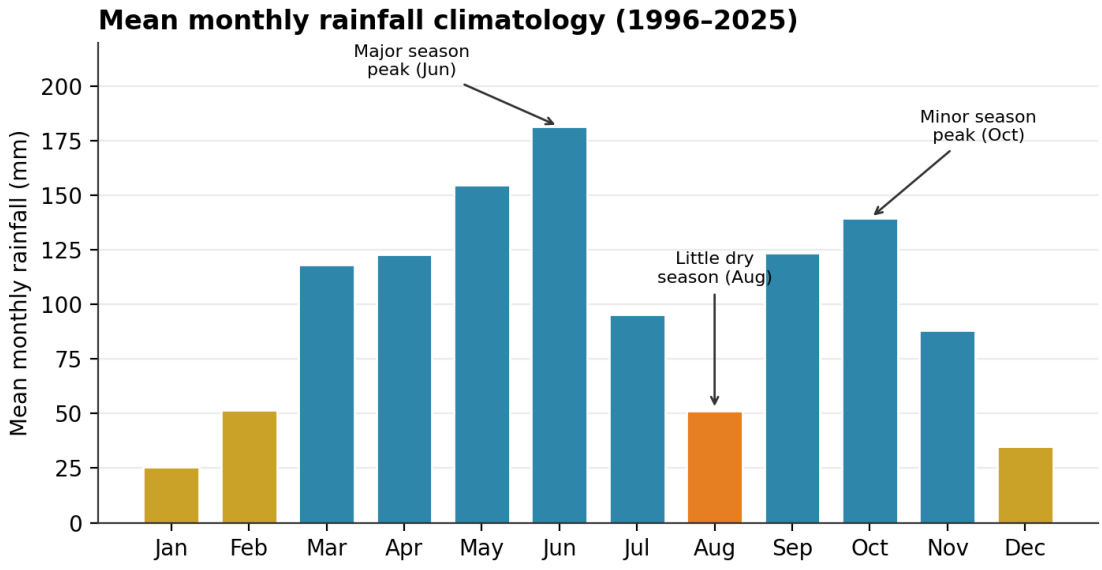


Figure 4. *Mean monthly rainfall (1996 to 2025) showing the bimodal regime: a major-season peak in June, the August little dry season, and a minor-season peak in October.*

3.3 Onset, cessation, and length of the rainy period

On average the major season opens around 5 March (day of year 64), but with a standard deviation of 18 days and a spread from as early as 1 February to as late as 22 April (Figure 5). Cessation is much steadier, clustering near 22 December with a standard deviation of 13 days, so the rainy period runs 292 days on average and between 247 and 333 days. Onset carries the strongest structural signal in the record, a drift toward earlier arrival of about 0.6 days per year, though it falls short of significance (Mann-Kendall p = 0.16, tau = -0.18). The direction is worth noting, because Lacombe et al. (2012) found the reverse across much of Ghana over 1960 to 2005, a delayed onset alongside lengthening dry spells at several stations. The reversal here fits the broader shift from mid-century deterioration to partial recovery after the 1990s (Nicholson 2013; De Longueville et al. 2016), the span this record covers. The bigger operational point is the variability itself. An 18-day standard deviation in onset means a planting decision keyed to a fixed date carries real risk in any single year, which is exactly the problem the agronomic onset criteria of Stern et al. (1982) were built to manage. Cessation, being stable, gives the harvest end of the calendar a firmer anchor than the start, the same asymmetry Amekudzi et al. (2015) found in their onset and cessation climatology across Ghana's agro-ecological zones.

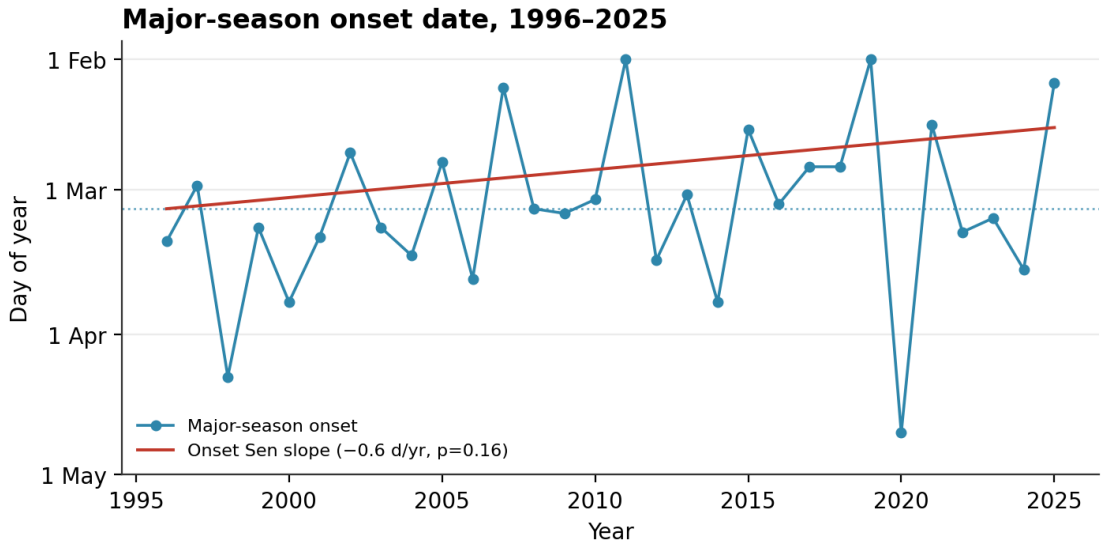


Figure 5. *Major-season onset date 1996 to 2025, with the long-term mean and the Sen's slope. The tendency toward earlier onset (about 0.6 days per year) is not statistically significant (p = 0.16).*

3.4 Dry spells within the rainy period

The annual longest run of consecutive dry days averages 24 and reaches 36 days in the most persistent year, with no trend. Within the March to November rainy period the station sees about 3.4 dry spells of a week or more each year and about 1.6 of ten days or more. The count of the long spells, those of at least ten days, edges down over the record (Mann-Kendall p = 0.05, tau = -0.24). That is the closest any series comes to significance, but with only thirty years behind it the result deserves caution. Its agronomic meaning is direct. Maize, the district's staple, is most vulnerable to water stress during tasselling and silking, a window of about two weeks around flowering, and a dry spell of ten days or more falling in that window is a leading cause of yield loss in rain-fed systems (Stern et al. 1982; Usman and Reason 2004). Fewer such spells therefore points to a modest easing of the single most damaging within-season hazard for the main crop. It also runs against the lengthening dry spells Lacombe et al. (2012) flagged as a national concern for the earlier period, and sits comfortably with the dry-season wetting Ackom et al. (2020) observed in the neighbouring Odaw basin. In practical terms, mid-season moisture risk at Somanya looks stable to slightly improving. The roughly three week-long and one-and-a-half longer spells that still occur every year mean staggered planting, drought-tolerant varieties, and small on-farm water storage remain worthwhile insurance in any given season.

3.5 Extreme rainfall indices and return periods

None of the ETCCDI extreme indices shows a statistically significant trend (Table 2, Figure 6). Annual maximum one-day rainfall averages 29.5 mm and the maximum five-day total 64.5 mm, both essentially stationary. Heavy-day counts stay modest, about 45 days a year at or above 10 mm but only about 5 at or above 20 mm, which describes frequent moderate rain rather than rare violent downpours (Zhang et al. 2011). The very-wet-day total (R95p) and the count of days at or above 20 mm both edge upward without reaching significance. A slight, unconfirmed intensification of heavy rainfall of this kind lines up with the significant rise in daily-maximum rainfall Ackom et al. (2020) detected for the Odaw basin, and with the broader expectation of increasing rainfall extremes across West Africa under warming (De Longueville et al. 2016; Nicholson 2013). Working with ten ETCCDI indices over Ghana from CHIRPS, Atiah et al. (2020) placed the minimum of the intensity indices over the north-western and eastern coasts, which is consistent with the modest extreme values recorded at Somanya on the inland edge of that coastal belt. The distinction matters for flood risk,

because it is heavy daily totals, not annual sums, that drive the urban and peri-urban flooding documented around Accra (Ansah et al. 2020; Ackom et al. 2020).

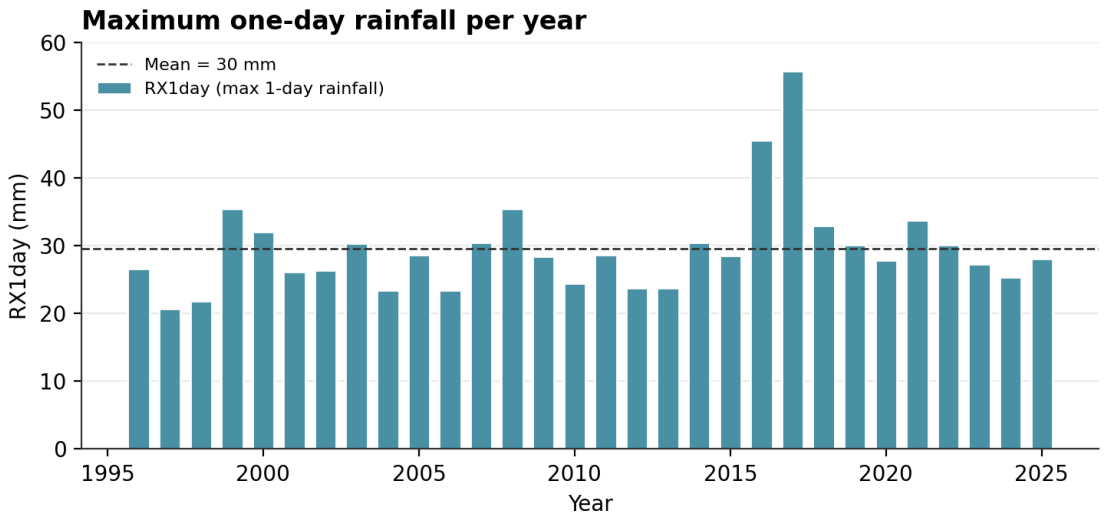


Figure 6. *Annual maximum one-day rainfall (RX1day) at Somanya with the long-term mean of 30 mm. The series shows no significant trend.*

To put these extremes in design terms, a Gumbel (type I extreme value) distribution and a generalized extreme value distribution were fitted to the 30 annual maxima, with 90 percent confidence intervals from bootstrap resampling (Figure 7). The Gumbel fit passes the Kolmogorov-Smirnov test ($D = 0.12$, $p = 0.77$). The well-constrained estimates, the ones within or close to the observed record, are a 2-year daily rainfall of about 28 mm (90 percent CI 27 to 30), a 5-year of 33 mm (31 to 37), a 10-year of 37 mm (33 to 41), and a 25-year of 41 mm (36 to 46), following Coles (2001). With only thirty annual maxima to work from, the 50 and 100-year levels, nominally about 44 and 47 mm, are uncertain extrapolations well beyond the record; their confidence intervals span 39 to 50 mm and 41 to 54 mm and should be read as indicative only. The shorter return levels give local drainage and small-structure design a station-specific footing, and complement the intensity-duration-frequency work called for in the flood-prone basins around Accra (Ackom et al. 2020). The observed 2017 maximum of 55.8 mm sits above even the central 100-year estimate, which marks it as a genuinely rare event in this record.

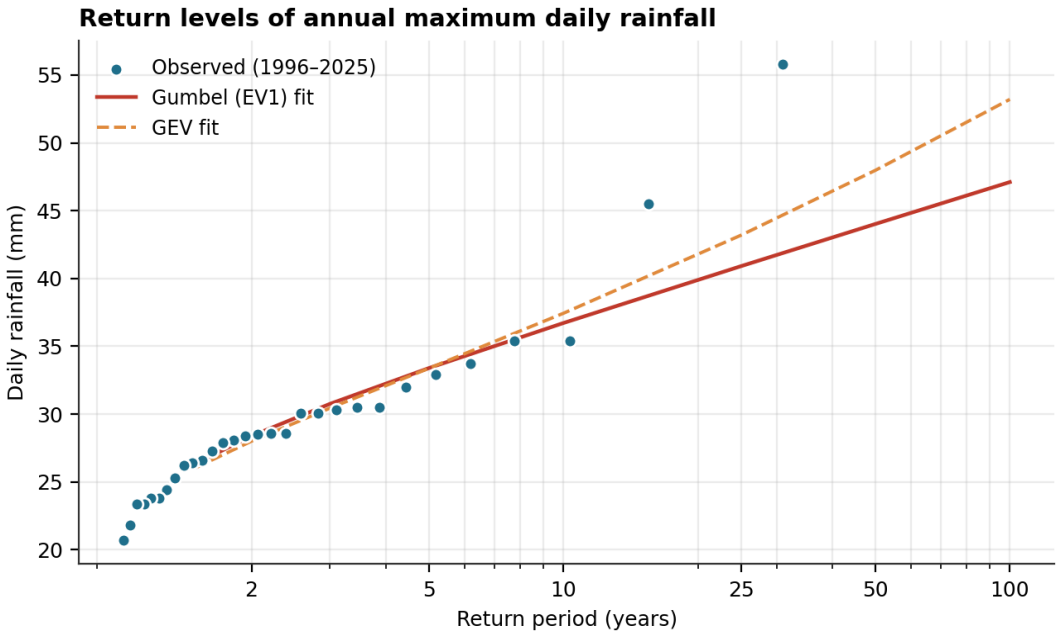


Figure 7. *Return levels of annual maximum daily rainfall at Somanya, with observed values (Weibull plotting position) and fitted Gumbel and GEV distributions. Uncertainty grows rapidly beyond the 25-year level.*

3.6 Meteorological drought

The 12-month SPI (Figure 8) tracks the wet and dry phases of the record cleanly. The driest stretches fall in the late 1990s and, most sharply, in 2015 to 2016, while 2008 stands out as the wettest year, followed by 2011, 2019, and 2017. Although 2005 posted the lowest single-year total (Section 3.1), the SPI works on accumulated departures over a moving window rather than calendar-year sums, and it flags 2015 to 2016 as the deepest, most sustained drought. Across the full 12-month series, moderate drought or worse (SPI at or below -1.0) turns up in roughly one month in six, severe drought in about one in twenty, and extreme drought only rarely, close to the frequencies McKee et al. (1993) associated with a well-behaved index. Shorter accumulation scales record more frequent but briefer excursions, the 3-month index reaching the most extreme single values, as expected when the averaging window narrows. The 2015 to 2016 dry phase coincides with a strong El Nino and with the flood-and-drought volatility widely reported for those years in Ghana (Ansah et al. 2020), a reminder that the SPI catches event-scale stress that annual totals can mask. No accumulation scale trends toward more frequent or deeper drought, consistent with the absence of any negative trend in the annual total and with the mild recovery signalled in the regional literature (Nicholson 2013; Ackom et al. 2020).

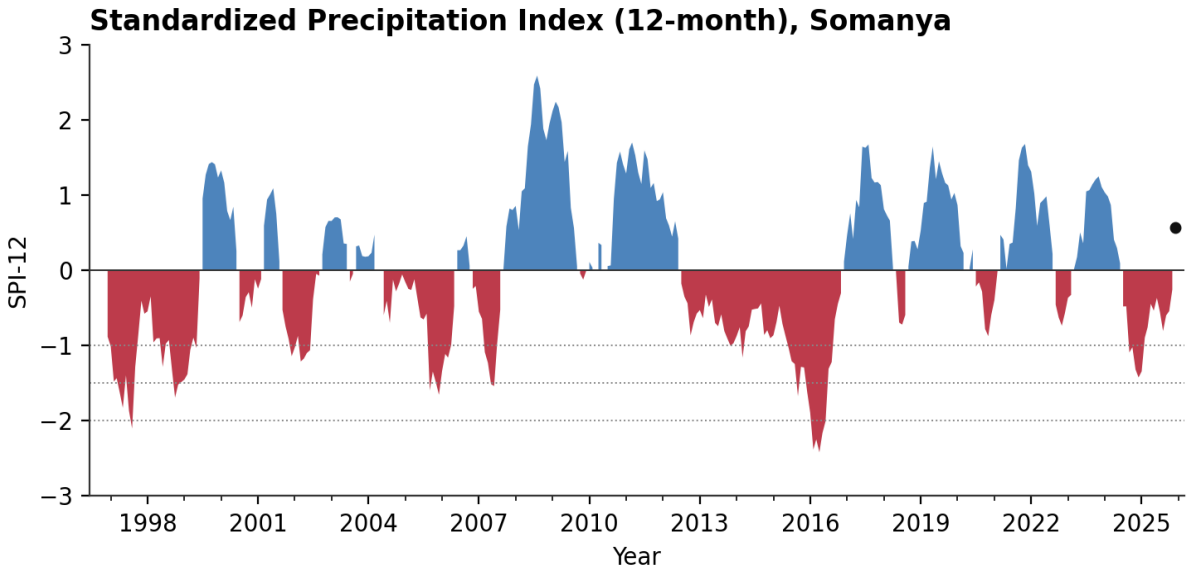


Figure 8. *Standardized Precipitation Index at the 12-month scale 1996 to 2025. Blue denotes wetter-than-normal and red drier-than-normal conditions. The driest phases are the late 1990s and 2015 to 2016; the wettest is 2008.*

3.7 Trend, homogeneity, and robustness

Table 2 gathers the trend testing for every series. The pattern is consistent: no significant trend, but a weak positive lean in the annual and seasonal totals and in several heavy-rainfall indices. The Sen's slope for the annual total is +2.75 mm per year, matched by the ordinary least squares fit (+2.49 mm per year, $R^2 = 0.03$), and decadal means climb from 1,137 mm in 1996 to 2005 to 1,226 mm in 2016 to 2025. Both season-structure signals, earlier onset and fewer long dry spells, concern the shape of the year rather than its total. The Pettitt test put its most likely break in 2006 but could not confirm it ($p = 0.68$), so the series is homogeneous, in line with the homogeneous Odaw records Ackom et al. (2020) reported for the same climatic zone.

Table 2. Mann-Kendall and Sen's slope results across all series. Only dry spells of ten days or more approach the 5 percent threshold; the annual result is unchanged under the Hamed and Rao (1998) correction.

Series / index	Sen's slope	Kendall τ	Z	p
Annual total	+2.75 mm/yr	0.13	0.96	0.34
Rainy days (≥1 mm)	+0.40 d/yr	0.16	1.22	0.22

Series / index	Sen's slope	Kendall τ	Z	p
SDII intensity	−0.001 mm/yr	−0.02	−0.11	0.91
Major season (Mar–Jul)	+0.62 mm/yr	0.04	0.32	0.75
Minor season (Aug–Nov)	+0.29 mm/yr	0.03	0.25	0.80
Onset date	−0.60 d/yr	−0.18	−1.39	0.16
Rainy-period length	+0.39 d/yr	0.09	0.68	0.50
Dry spells ≥10 d	−0.00 /yr	−0.24	−1.95	0.05
RX1day	+0.14 mm/yr	0.16	1.21	0.22
RX5day	−0.01 mm/yr	0.00	0.00	1.00
R20mm	+0.08 d/yr	0.20	1.56	0.12
R95p	+1.68 mm/yr	0.15	1.14	0.25

Serial correlation does not explain these results. Lag-1 autocorrelation of the annual series is effectively zero (-0.01), and the variance-corrected modified Mann-Kendall test of Hamed and Rao (1998) returns the same answer as the original ($p = 0.34$). That check matters, because near-significant results in hydrological series can be artefacts of autocorrelation (Hamed and Rao 1998); here it confirms the original conclusion rather than overturning it. Set against the wider record, the weak positive lean at Somanya is very much in step with recent southern-Ghana work. Ackom et al. (2020) found a non-significant annual increase of 3.7 mm per year in the Odaw basin, of the same order as the 2.75 mm per year here; Braimah et al. (2022) found rising minor-season rainfall at sixteen of seventeen southern stations; Logah et al. (2013) noted a slight increase over Accra in recent decades; and Nyatuame et al. (2014) and Kabo-Bah et al. (2016) reported mostly weak or non-significant trends elsewhere in the country. Taken together, this suggests the mid-century drying documented by Lacombe et al. (2012) and Owusu and Waylen (2009) has given way to a gradual, spatially coherent recovery in the south, part of the wider West African rainfall recovery since the 1990s (Sanogo et al. 2015; Nicholson 2013). The Ghana Meteorological Agency (2024) sets such year-to-year departures against the 1991 to 2020 normal, a reminder that this gentle positive tendency coexists with substantial interannual variability.

Because the Mann-Kendall test can miss a trend confined to the low or high range of a variable, the annual series was also run through the innovative trend analysis of Sen (2012), which plots the sorted first half of the record against the sorted second half and reads trend from how far the points fall off the 1:1 line (Figure 9). The points cluster tightly on the line, giving an innovative trend slope of essentially zero (-0.14 mm per year); the lowest annual totals rise a little in the second half while the highest fall a little, but neither shift is material. The innovative trend analysis therefore backs the Mann-Kendall result of no meaningful change in the annual total, and it tempers the weak positive trend by showing that the highest totals, the ones most relevant to flooding, are not increasing.

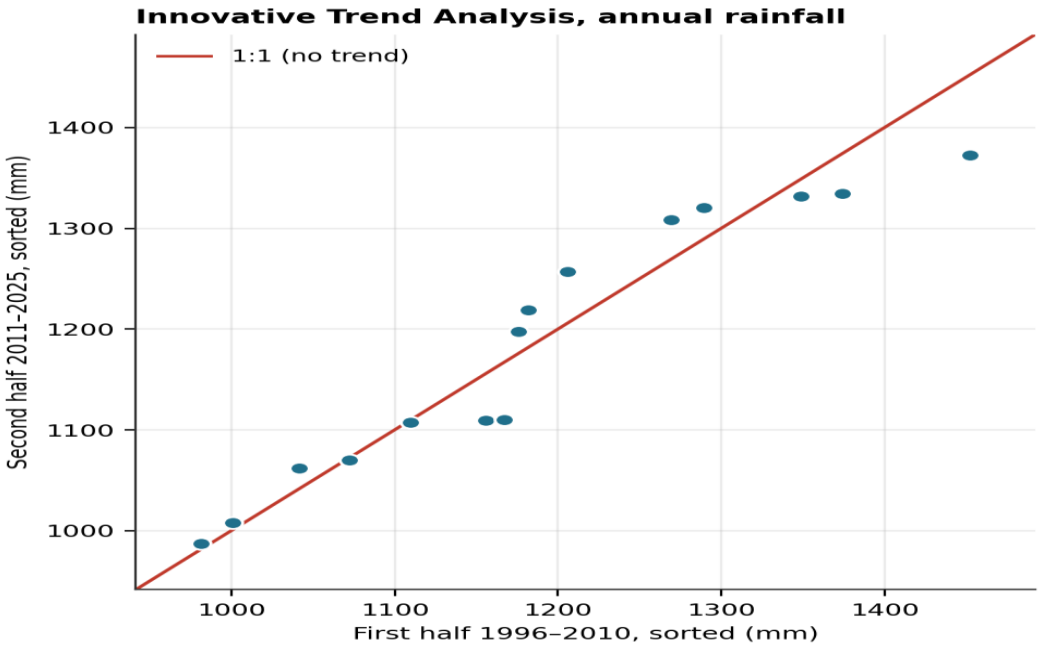


Figure 9. *Innovative trend analysis of annual rainfall (Sen 2012). Points on the 1:1 line indicate no trend; the tight clustering confirms a near-stationary series.*

3.8 Gauge validation and spatial representativeness

The central question for any single-gauge study is whether the record speaks for its surroundings or only for one point. Compared with CHIRPS for the Somanya grid cell, agreement improves as the averaging window widens (Table 3, Figure 10). Day to day, the two series correlate moderately (Pearson r = 0.67, r^2 = 0.44), which is expected, since a 5.5 km satellite estimate cannot resolve the exact timing and footprint of individual convective cells (Dinku et al. 2018). Aggregate away the daily noise and agreement climbs: monthly totals correlate strongly (r = 0.90, r^2 = 0.81) and annual totals well (r = 0.69). At all three scales CHIRPS runs about 5 percent wet (PBIAS +5.0 percent),

overestimating the annual total by roughly 59 mm. On the thresholds of Moriasi et al. (2007), an absolute PBIAS below 10 percent rates as very good, so gauge and independent gridded product are in strong systematic agreement. The monthly climatologies track closely, parting company most in October, where CHIRPS is about 28 mm wetter, a known habit of satellite products on the Guinea coast, where they overestimate the minor-season peak (Dinku et al. 2018). CHIRPS also picks up fewer wet days than the gauge (3,454 against 4,354), the familiar trouble satellite retrievals have with light rainfall, yet it still agrees on the wet-or-dry state of 83 percent of days. This is the level of gauge-to-satellite consistency Dinku et al. (2018) reported for well-behaved stations in the region, and it confirms the record as a sound and representative basis for the station-scale results reported above.

Table 3. Agreement between the Somanya gauge and CHIRPS at three temporal scales. PBIAS below 10 percent is very good by the criteria of Moriasi et al. (2007).

Scale	Pearson r	r^2	PBIAS	RMSE
Daily (n = 10,958)	0.67	0.44	+5.0 %	5.2 mm
Monthly (n = 360)	0.90	0.81	+5.0 %	30.1 mm
Annual (n = 30)	0.69	0.48	+5.0 %	149 mm

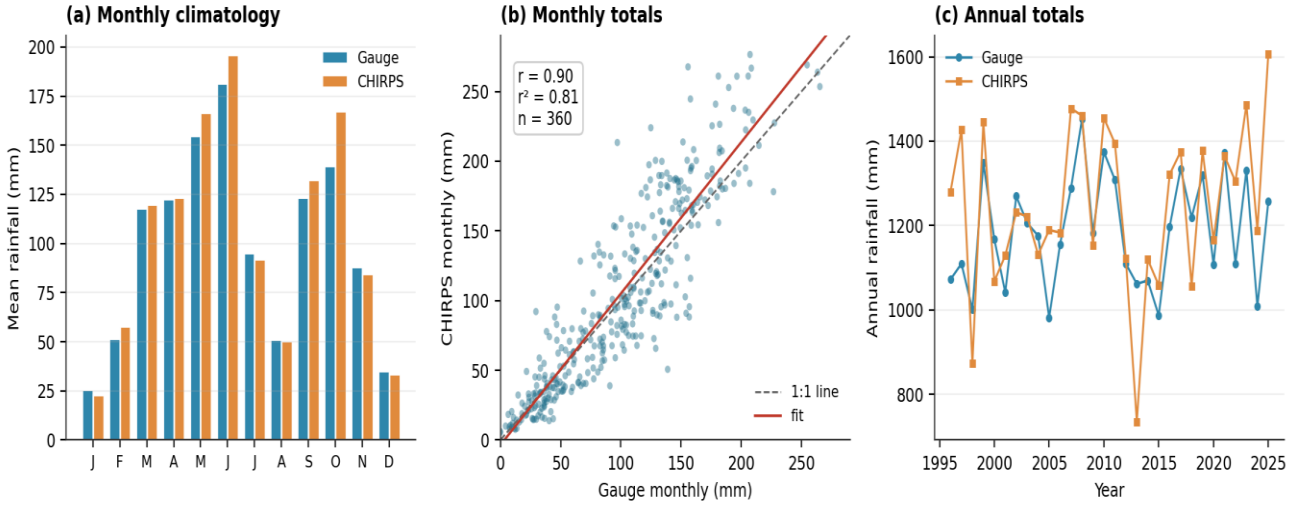


Figure 10. *Validation of the Somanya gauge against CHIRPS 1996 to 2025: (a) monthly climatology, (b) monthly totals with the 1:1 line and least-squares fit, and (c) annual totals. Agreement is strongest at the monthly scale (r = 0.90).*

Widening the CHIRPS comparison from the single Somanya pixel to a grid of ninety pixels across the surrounding district, a box of roughly 50 km, sets the gauge in its spatial context (Figure 11). Grid-mean annual rainfall is 1,193 mm, within 6 mm of the gauge mean of 1,187 mm, and the gauge value sits near the middle of the local distribution, at about the 39th percentile. The single station is therefore representative of the district average rather than an outlier, which is the assumption most single-gauge studies make but rarely test (Owusu and Waylen 2009; Dinku et al. 2018). Across the grid, rainfall runs from about 910 mm to 1,369 mm, a spread of 459 mm, yet its spatial coefficient of variation is only 9.8 percent, close to the 11.1 percent interannual variability of the gauge, so the district is about as variable across space as the station is from year to year. The dominant pattern is a strong west-to-east gradient (correlation with longitude r = -0.83): the wettest pixels lie to the north-west, inland toward the forest margin, and the driest to the south-east, toward the drier Accra plains and coast. This is the expected expression of the coastal-savanna transition (Dickson and Benneh 1988), and it mirrors the highland-wet, lowland-dry contrast Ackom et al. (2020) mapped within the neighbouring Odaw basin. For district planning, the map implies that settlements to the south-east of Somanya face a meaningfully drier regime, by up to a few hundred millimetres a year, than the gauge alone would suggest.

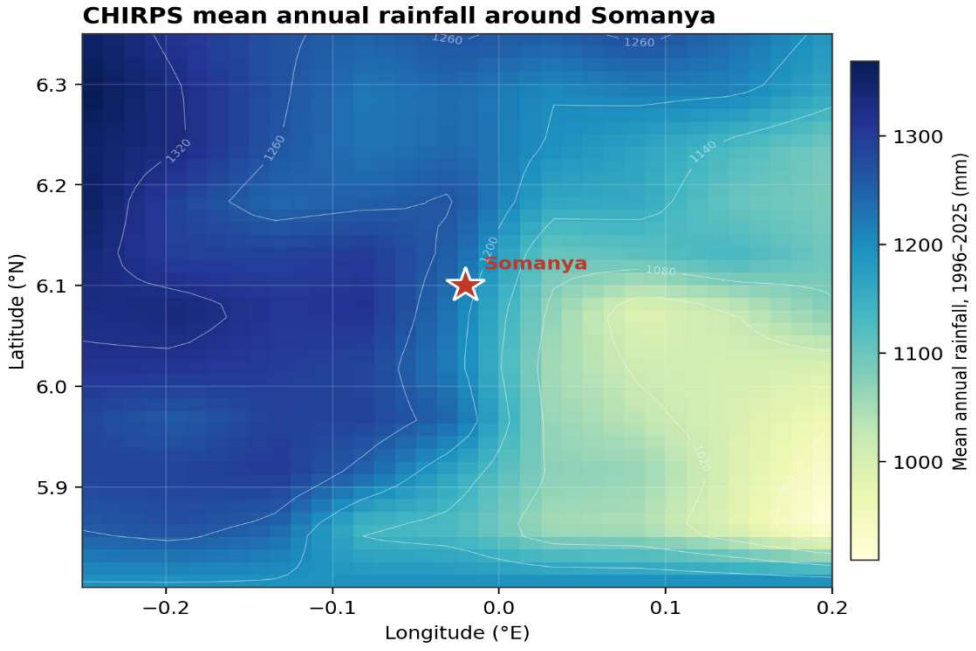


Figure 11. *CHIRPS mean annual rainfall (1996 to 2025) across a grid around Somanya (star). Rainfall decreases from the wetter inland north-west toward the drier south-east, and the gauge sits close to the district mean.*

3.9 Association with the El Nino-Southern Oscillation

Interannual rainfall at Somanya carries a modest but coherent imprint of the El Nino-Southern Oscillation (Table 4, Figure 12). Annual rainfall correlates negatively with the annual-mean Oceanic Nino Index (Pearson r = -0.33, p = 0.07): wetter years tend to fall in the cool La Nina phase and drier years in the warm El Nino phase. Grouping the thirty years by phase sharpens the picture. La Nina years averaged 1,293 mm, about 105 mm above the long-term mean and roughly 150 mm above the neutral-year mean of 1,142 mm, while El Nino years fell in between at 1,204 mm. A one-way analysis of variance across the three phases is significant (F = 4.05, p = 0.03), so the phase differences are unlikely to be chance. The direction matches the established mechanism by which La Nina strengthens, and El Nino weakens, the West African monsoon through shifts in the Walker circulation and the tropical Atlantic response (Joly and Voldoire 2009; Nicholson 2013). It also holds up locally: Atiah et al. (2020) found significant negative correlations between the NINO3.4 index and wet rainfall indices over west-central Ghana, the same sign of association recorded here. The El Nino composite is the noisiest of the three, since only five strong-enough El Nino years fall in the record, and the very strong 1997 and 2015 events had mixed local expressions, so it should be read as indicative rather than definitive. Even so, the significant phase contrast suggests that ENSO phase can offer useful climatic context for anticipating an anomalously wet or dry year at Somanya, a signal that dovetails with the drought phases the SPI identified for 2015 to 2016.

Table 4. Composite annual rainfall by ENSO phase, classified by annual-mean Oceanic Nino Index 1996 to 2025. Differences are significant at the 5 percent level (one-way ANOVA, F = 4.05, p = 0.03).

ENSO phase	Years (n)	Mean (mm)	Anomaly (mm)
El Nino (ONI ≥ +0.5)	5	1,204	+16
Neutral	18	1,142	−45

La Nina (ONI ≤ −0.5)	7	1,293	+105

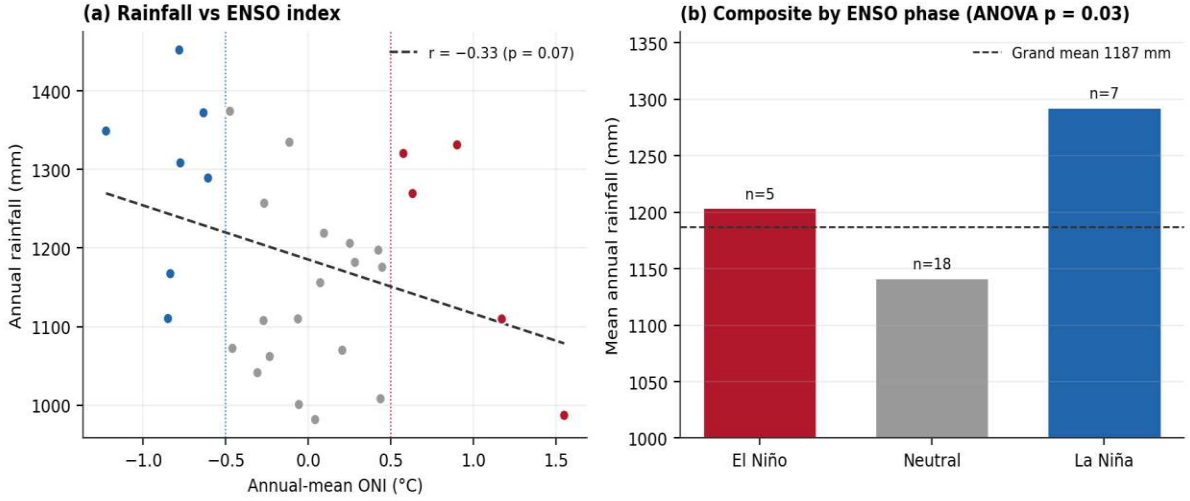


Figure 12. *Association between annual rainfall and ENSO: (a) rainfall against the annual-mean Oceanic Nino Index, with El Nino (red), neutral (grey), and La Nina (blue) years; (b) composite annual rainfall by ENSO phase (one-way ANOVA p = 0.03).*

3.10 Implications and limitations

Put together, the results describe a rainfall regime steady in amount but quietly changing in structure, and that distinction shapes how local adaptation should be framed. Regional projections expect greater variability and heavier extremes across West Africa as warming continues (IPCC 2021; Atiah et al. 2020), yet Somanya's recent record shows no such intensification, and if anything a mild easing of dry-season stress. The mismatch is itself informative. It shows the regional signal does not fall evenly on every district (Sanogo et al. 2015), and it warns against pulling basin or national trends straight into a local plan. For a rain-fed economy, the working message is to aim adaptation at season timing and dry-spell risk, the levers that actually move yields, rather than at the annual total, which here is dependable (Stern et al. 1982; Amekudzi et al. 2015).

Read as a whole, the results answer the study's questions coherently. Somanya's rainfall is dependable in total, bimodal and moderately seasonal in shape, and free of any significant long-term trend or abrupt change, while its season structure eases gently, with earlier onset and fewer long dry spells. For a district that plants twice a year this is a favourable baseline, but the practical risks lie in the shape of the year rather than its amount. The 18-day spread in onset complicates planting decisions in any single year (Stern et al. 1982); the 2015 to 2016 drought phase shows how event-scale stress

can strike a stable climate (Ansah et al. 2020); and the upward drift in heavy daily totals, though not yet significant, is the variable most relevant to local flooding (Ackom et al. 2020). The significant ENSO signal adds a further planning consideration, since the phase of the oscillation may offer useful context for anticipating an anomalously wet or dry season (Joly and Voldoire 2009).

Two limitations bound these conclusions. The first is that the analysis rests on one gauge. The CHIRPS grid (Section 3.8) shows that gauge to be representative of the district mean and maps the west-to-east gradient around it, which substantially addresses the usual single-station concern, but ground validation across that gradient would still benefit from a denser rain-gauge network (Owusu and Waylen 2009; Dinku et al. 2018). The second is length. A thirty-year window, though adequate for a climatological normal, has limited statistical power to separate a slow trend from strong interannual noise, which is part of why the positive slopes remain non-significant and why the near-significant dry-spell result should be treated as suggestive rather than settled.

4. Conclusion

This study set out to characterize the rainfall regime of Somanya over 1996 to 2025 from a complete daily record and to establish an agronomically relevant, independently validated baseline for the district, addressing six objectives. First, on the annual and seasonal regime, it found rainfall to be bimodal, moderately seasonal, and dependable, averaging 1,187 mm a year at a coefficient of variation of only 11 percent, with peaks in June and October around the August little dry season. Second, on season timing, it found that the major season opens on average in early March but with an 18-day spread, while the rainy period closes far more regularly near late December, so onset is the less predictable end of the calendar. Third, on dry spells, it found about 3.4 week-long and 1.6 ten-day-or-longer spells each rainy season, with a borderline decline in the longest spells. Fourth, on extremes, it found no significant trend in any ETCCDI index and estimated well-constrained design rainfalls of about 37 and 41 mm for the 10 and 25-year daily events. Fifth, on drought, the Standardized Precipitation Index identified 2015 to 2016 as the deepest sustained dry phase and 2008 as the wettest year, with no trend toward more frequent drought. Sixth, on trend, validation, and drivers, it found no significant trend or abrupt change in the annual series, a result robust to serial correlation and confirmed by innovative trend analysis; strong agreement between the gauge and CHIRPS at the monthly scale ($r = 0.90$); a west-to-east drying gradient within which the gauge represents the district mean; and a significant organisation of interannual rainfall by the El Nino-Southern Oscillation, La Nina years running markedly wetter than neutral years. Taken together, these

findings show a rainfall regime that is stable in amount but subtly shifting in structure, both structural signals, earlier onset and fewer long dry spells, favouring rain-fed farming. For the district the practical implications are concrete: planting should be keyed to the observed onset rather than a fixed calendar date, given the 18-day onset spread; mid-season dry-spell risk, though easing, still warrants staggered planting and drought-tolerant varieties; communities to the south-east of the gauge should plan for a drier regime and greater water-conservation need; and an established La Nina or El Nino state offers a useful early signal for seasonal outlooks. The study provides a validated baseline on which local agriculture and water management can build, and its approach is transferable to other data-scarce districts across the bimodal south.

Acknowledgements

The authors are grateful to the Ghana Meteorological Agency (GMet) for providing the daily rainfall record for Somanya. We also acknowledge the Climate Hazards Center, University of California, Santa Barbara, for the CHIRPS data, and the NOAA Climate Prediction Center for the Oceanic Nino Index.

References

Ackom EK, Adjei KA, Odai SN (2020) Spatio-temporal rainfall trend and homogeneity analysis in flood prone area: case study of Odaw river basin-Ghana. SN Applied Sciences 2:2141

552 Amekudzi LK, Yamba EI, Preko K, Asare EO, Aryee J, Baidu M, Codjoe SNA (2015) Variabilities
553 in rainfall onset, cessation and length of rainy season for the various agro-ecological zones of
554 Ghana. Climate 3:416–434

555 Ansah SO, Ahiataku MA, Yorke CK, Otu-Larbi F, Yahaya B, Lamptey PNL, Tanu M (2020)
556 Meteorological analysis of floods in Ghana. Advances in Meteorology 2020:4230627

557 Atiah WA, Mengistu Tsidu G, Amekudzi LK, Yorke C (2020) Trends and interannual variability of
558 extreme rainfall indices over Ghana, West Africa. Theoretical and Applied Climatology
559 140:1393–1407

560 Awotwi A, Anornu GK, Quaye-Ballard J, Annor T, Forkuo EK (2017) Analysis of climate and
561 anthropogenic impacts on runoff in the Lower Pra River Basin of Ghana. Heliyon 3:e00477

562 Baidu M, Amekudzi LK, Aryee JNA, Annor T (2017) Assessment of long-term spatio-temporal
563 rainfall variability over Ghana using wavelet analysis. Climate 5:30

564 Braimah M, Asante VA, Ahiataku MA, Ansah SO, Otu-Larbi F, Yahaya B, Ayabilah JB, Nkrumah
565 F (2022) Variability of the minor season rainfall over southern Ghana (1981 to 2018). Advances
566 in Meteorology 2022:1861130

567 Coles S (2001) An Introduction to Statistical Modeling of Extreme Values. Springer, London

568 De Longueville F, Hountondji YC, Kindo I, Gemenne F, Ozer P (2016) Long-term analysis of rainfall
569 and temperature data in Burkina Faso (1950 to 2013). International Journal of Climatology
570 36:4393–4405

571 Dickson KB, Benneh G (1988) A New Geography of Ghana. Longman, London

572 Dinku T, Funk C, Peterson P, Maidment R, Tadesse T, Gadain H, Ceccato P (2018) Validation of the
573 CHIRPS satellite rainfall estimates over eastern Africa. Quarterly Journal of the Royal
574 Meteorological Society 144:292–312

575 Funk C, Peterson P, Landsfeld M, Pedreros D, Verdin J, Shukla S, Husak G, Rowland J, Harrison L,
576 Hoell A, Michaelsen J (2015) The climate hazards infrared precipitation with stations: a new
577 environmental record for monitoring extremes. Scientific Data 2:150066

578 Ghana Meteorological Agency (2024) 2024 State of the Climate, Ghana. GMet, Accra

579 Hamed KH, Rao AR (1998) A modified Mann-Kendall trend test for autocorrelated data. Journal of
580 Hydrology 204:182–196

IPCC (2021) Climate Change 2021: The Physical Science Basis. Contribution of Working Group I to the Sixth Assessment Report of the Intergovernmental Panel on Climate Change. Cambridge University Press, Cambridge and New York

Joly M, Voldoire A (2009) Influence of ENSO on the West African monsoon: temporal aspects and atmospheric processes. Journal of Climate 22:3193–3210

Kabo-Bah AT, Diji CJ, Nokoe K, Mulugetta Y, Obeng-Ofori D, Akpoti K (2016) Multiyear rainfall and temperature trends in the Volta River basin and their potential impact on hydropower generation in Ghana. Climate 4:49

Kendall MG (1975) Rank Correlation Methods, 4th ed. Charles Griffin, London

Lacombe G, McCartney M, Forkuor G (2012) Drying climate in Ghana over the period 1960 to 2005: evidence from the resampling-based Mann-Kendall test at local and regional levels. Hydrological Sciences Journal 57:1594–1609

Logah FY, Obuobie E, Ofori D, Kankam-Yeboah K (2013) Analysis of rainfall variability in Ghana. International Journal of Latest Research in Engineering and Computing 1:1–8

Mann HB (1945) Nonparametric tests against trend. Econometrica 13:245–259

McKee TB, Doesken NJ, Kleist J (1993) The relationship of drought frequency and duration to time scales. Proceedings of the 8th Conference on Applied Climatology, American Meteorological Society, 179–184

Moriasi DN, Arnold JG, Van Liew MW, Bingner RL, Harmel RD, Veith TL (2007) Model evaluation guidelines for systematic quantification of accuracy in watershed simulations. Transactions of the ASABE 50:885–900

Nicholson SE (2013) The West African Sahel: a review of recent studies on the rainfall regime and its interannual variability. ISRN Meteorology 2013:453521

NOAA Climate Prediction Center (2024) Oceanic Nino Index (ONI). National Oceanic and Atmospheric Administration, National Weather Service, College Park, MD

Nyatuame M, Owusu-Gyimah V, Ampiaw F (2014) Statistical analysis of rainfall trend for Volta region in Ghana. International Journal of Atmospheric Sciences 2014:203245

Ofori-Sarpong E, Annor J (2001) Rainfall over Accra 1901 to 1990. Weather 56:55–62

Oliver JE (1980) Monthly precipitation distribution: a comparative index. The Professional Geographer 32:300–309

Omotosho JB, Abiodun BJ (2007) A numerical study of moisture buildup and rainfall over West Africa. Meteorological Applications 14:209–225

Owusu K, Waylen PR (2009) Trends in spatio-temporal variability in annual rainfall in Ghana (1951 to 2000). Weather 64:115–120

Pettitt AN (1979) A non-parametric approach to the change-point problem. Journal of the Royal Statistical Society, Series C 28:126–135

Quaye-Ballard JA, Okrah TM, Andam-Akorful SA, Awotwi A, Antwi T, Osei-Wusu W, Quaye-Ballard NL (2020) Spatiotemporal dynamics of rainfall in Upper East Region of Ghana, West Africa 1981 to 2016. SN Applied Sciences 2:1–12

Sanogo S, Fink AH, Omotosho JA, Ba A, Redl R, Ermert V (2015) Spatio-temporal characteristics of the recent rainfall recovery in West Africa. International Journal of Climatology 35:4589–4605

Sen PK (1968) Estimates of the regression coefficient based on Kendall's tau. Journal of the American Statistical Association 63:1379–1389

Sen Z (2012) Innovative trend analysis methodology. Journal of Hydrologic Engineering 17:1042–1046

Stern RD, Dennett MD, Dale IC (1982) Analysing daily rainfall measurements to give agronomically useful results. Experimental Agriculture 18:223–236

Usman MT, Reason CJC (2004) Dry spell frequencies and their variability over southern Africa. Climate Research 26:199–211

Walsh RPD, Lawler DM (1981) Rainfall seasonality: description, spatial patterns and change through time. Weather 36:201–208

Zhang X, Alexander L, Hegerl GC, Jones P, Klein Tank A, Peterson TC, Trewin B, Zwiers FW (2011) Indices for monitoring changes in extremes based on daily temperature and precipitation data. WIREs Climate Change 2:851–870

Statements and Declarations

Funding

This research received no specific grant from any funding agency in the public, commercial, or not-for-profit sectors.

Competing interests

The authors declare that they have no known competing financial interests or personal relationships that could have appeared to influence the work reported in this paper.

Author contributions

M.A. conceived and designed the study, curated the data, carried out the statistical analysis, and wrote the original draft.

J.A. and B.A. contributed to the methodology, interpretation of the results, and review and editing of the manuscript.

F.E. contributed to the conceptual framing, supervision, and critical review of the manuscript.

S.O.K (Sarfo Okyere Kore) Review and editing of the manuscript, interpretation of results, and contribution to the overall scientific refinement of the study.

M.S.D (Maximillian-Robert Selorm Doku) contributed to Methodological guidance, interpretation of results, critical review, and editing of the manuscript.

Data availability

The daily rainfall record for Somanya (1996 to 2025) was obtained from the Ghana Meteorological Agency (GMet) and is available from GMet on reasonable request, subject to the Agency's data-sharing policy. The CHIRPS version 2.0 data (Funk et al. 2015) are openly available from the Climate Hazards Center, and the Oceanic Nino Index from the NOAA Climate Prediction Center. All indices were computed from the gauge record without gap-filling, since the series is complete; the analysis code is available from the corresponding author on request.